ADVANCED MATERIALS

DOI: 10.1002/adma.200801319

3D Cell-Migration Studies using Two-Photon Engineered Polymer Scaffolds**

By *Prakriti Tayalia, Cleber R. Mendonca, Tommaso Baldacchini, David J. Mooney,* and *Eric Mazur**

Recent research reveals intriguing differences between cell migration in two and three dimensions. Studies of cell migration are important for understanding a variety of physiological and pathological processes such as embryonic development, cancer metastasis, blood vessel formation and remodeling, tissue regeneration, immune surveillance, and inflammation.[1] Researchers have extensively studied the mechanisms and regulation of cell migration in two-dimensional (2D) cell-culture models, where migration is predominantly a function of adhesion and de-adhesion events and where there are no spatial barriers to the advancing cell body.[2,3] However, discrepancies between the behavior of cells in culture (2D) and in vivo (3D) indicate it is important to use 3D models to better represent the microenvironment of living tissues with respect to dimensionality, architecture and cell polarity. Unlike cells migrating in 2D, cells in 3D need to overcome the physical resistance provided by the matrix, change shape and morphology, or enzymatically degrade matrix components.[1,4–6]

Fibrous matrices like collagen, matrigel and fibrinogen derived from tissue are widely used for studying 3D cell migration in vitro.[6–8] 3D cell tracking has also been done in vivo in live zebrafish embryos.[9] The natural matrices used for in vitro studies are inherently adhesive and have random pore and mesh sizes. However, these matrices do not allow control of adhesion, matrix architecture, and mechanical stiffness, and thus it is difficult to determine the effect of each of these parameters on cell migration. Synthetic matrices provide greater control over material properties and cell behavior to provide insight into the complexity of cell-signaling mechanisms. Although techniques like soft lithography, photolithography, and microprinting have been extensively used to study cell behavior on 2D patterned substrates,[10,11] few tools exist for studying cells in a well-controlled 3D environment. Current fabrication techniques for 3D porous scaffolds, such as solvent casting/particulate leaching, gas foaming, and phase inversion, do not permit precise control of pore size, of pore geometry, and of the spatial distribution of pores, nor is it possible to construct internal channels within the scaffold.[12–17] Rapid prototyping of scaffolds allows control of complex internal features of scaffolds, but the resolution and smallest feature size is usually constrained by the process parameters and properties of the building materials. For most of the rapid prototyping techniques currently used to fabricate scaffolds, the smallest pore size is about 50–100 μm.[13,18] Powder-based techniques, such as three-dimensional printing (3DP) and selective laser sintering (SLS), are not suitable for cell studies because it is difficult to remove material trapped in the scaffold structures. Thus, matrices obtained by conventional scaffold fabrication techniques do not provide the precision required to control and understand cell attachment and migration in a 3D environment. Recently, two-photon polymerization was used to create ossicular replacement prostheses and other medical devices with a larger range of sizes, shapes and materials than previously demonstrated with other microfabrication techniques.[19]

We use two-photon polymerization to precisely control the pore size of a 3D matrix. The technique permits control of architectural parameters like pore size, shape, porosity and permeability down to the submicrometer scale. It is also possible to control the presentation of biochemical and biophysical cues in the matrix to study cell function. We could present different cues by using materials with different mechanical properties or by modifying the material with specific or non-specific cell adhesion peptides. Lutolf et al. have demonstrated that modification of acrylate hydrogels with peptides can be readily achieved.[20] In this paper we present standard protocols for microfabrication and cell culture, a three-dimensional imaging technique and quantitative analysis method for studying 3D cell migration, and compare cell migration in 2D and 3D.

[*] Prof. E. Mazur, Prof. D. J. Mooney, P. Tayalia
School of Engineering and Applied Sciences, Harvard University
9 Oxford Street, Cambridge, Massachusetts 02138 (USA)
E-mail: mazur@seas.harvard.edu
Dr. C. R. Mendonca
Instituto de Física de São Carlos, Universidade de São Paulo
Caixa Postal 369, 13560-970 São Carlos, SP (Brazil)
Dr. T. Baldacchini
Technology and Applications Center, Newport Corporation
1791 Deere Avenue, Irvine, CA 92606 (USA)

[**] Several people contributed to the work described in this paper. P.T. conceived of the basic idea for this work, designed and carried out the experiments, and analyzed the results. T.B. provided expertise on two-photon polymerization and polymer chemistry. C.M. assisted with the experiments. D.M. and E.M. supervised the research, analysis of the data, and the development of the manuscript. P.T. wrote the first draft of the manuscript; all authors subsequently took part in the revision process and approved the final copy of the manuscript. M. Winkler, J. Dowd and C. Evans provided feedback on the manuscript throughout its development. The research described in this paper was supported by the NSF-sponsored Materials Research Science and Engineering Center under contract DMR-0213805 and NIH under contract R37 DE013033. Supporting Information is available online from Wiley InterScience or from the author.

Three-dimensional microfabrication by two-photon polymerization takes advantage of the spatial selectivity of two-photon absorption[21] to fabricate 3D polymeric structures of any shape and size with submicrometer resolution.[22,23] The nonlinear nature of the two-photon absorption process confines the photopolymerization to the focal volume. In the current work, we use a viscous triacrylate two-monomer composition for the fabrication of scaffolds.[24] This monomer is transparent at the laser wavelength of 800 nm, so that it cross-links only within the focal region where nonlinear absorption occurs. Figure 1a shows a schematic of the set-up. A 76-MHz train of 120-fs laser pulses of 800-nm wavelength is focused through a microscope objective in to the sample. The focal point of the laser beam is translated in the sample to create complex three-dimensional patterns. After the laser exposure is completed, we wash away the unexposed resin with a solvent, leaving behind the 3D interconnected scaffolds fabricated for the current study.

The scaffolds used in this study are interconnected woodpile structures having alternate layers of orthogonal beams in the z-direction (Fig. 1b). Figure 1b defines various parameters of the scaffold design. The pores are square in shape and permit fluid flow and migration of cells. We used four different lateral pore sizes in this study: A = 12, 25, 52 and 110 μm. This range of pore size spans from a little below the size of a single cell (approximately 15 μm) to ten times the cell size. The lateral beam size is kept fixed at B = 5 μm and the z-distance between parallel beams is kept fixed at C = 12 μm for all scaffolds. The height and width of each scaffold is D = 100 μm and E = 350 μm, respectively. Figure 1c is a top view of a 1.75-mm long and 350-μm wide scaffold with a 110-μm pore size. Figure 1d shows a similar scaffold with a 52-μm pore size. Figures 1e and 1f are side views of scaffolds with 25-μm and 52-μm pore sizes, respectively.

We measured the mechanical properties of the photopolymerized triacrylate, from which the scaffolds are fabricated, and confirmed its biocompatibility for cell growth. Using methanol as a solvent, we leach out the unpolymerized monomer from the polymer. After the leaching, we seeded the substrate with cells and observed the cell number to increase (Figs. 1g, 1h), confirming the material to be compatible for cell attachment and cell growth. Figure 1i shows the bulk mechanical stiffness of the polymer after UV photopolymerization as a function of composition of the two monomers in the triacrylate system, before and after solvent leaching. The leaching process does not affect the elastic modulus of the polymer, and the elastic modulus of the polymer system can be varied from 0.1 GPa to 1.2 GPa. This range of values is in agreement with the elastic modulus of microcantilevers prepared by two-photon polymerization of the same monomer mixture.[25] Thus, regardless of the polymerization process, the polymerized material has similar mechanical properties. We confirmed biocompatibility over the entire range of compositions shown in Fig. 1i.

We studied cell migration in the scaffolds using the human fibrosarcoma cell line HT1080. To minimize photobleaching and the light-induced phototoxic effects of commercially available artificial dyes, we fluorescently labeled the cells by transfecting them with green fluorescent protein (GFP) plasmid. We confirmed that the transfection process does not affect cell motility by comparing cell migration of transfected and untransfected cells. The GFP-labeling permits 3D imaging of cells inside scaffolds using confocal microscopy and also allows

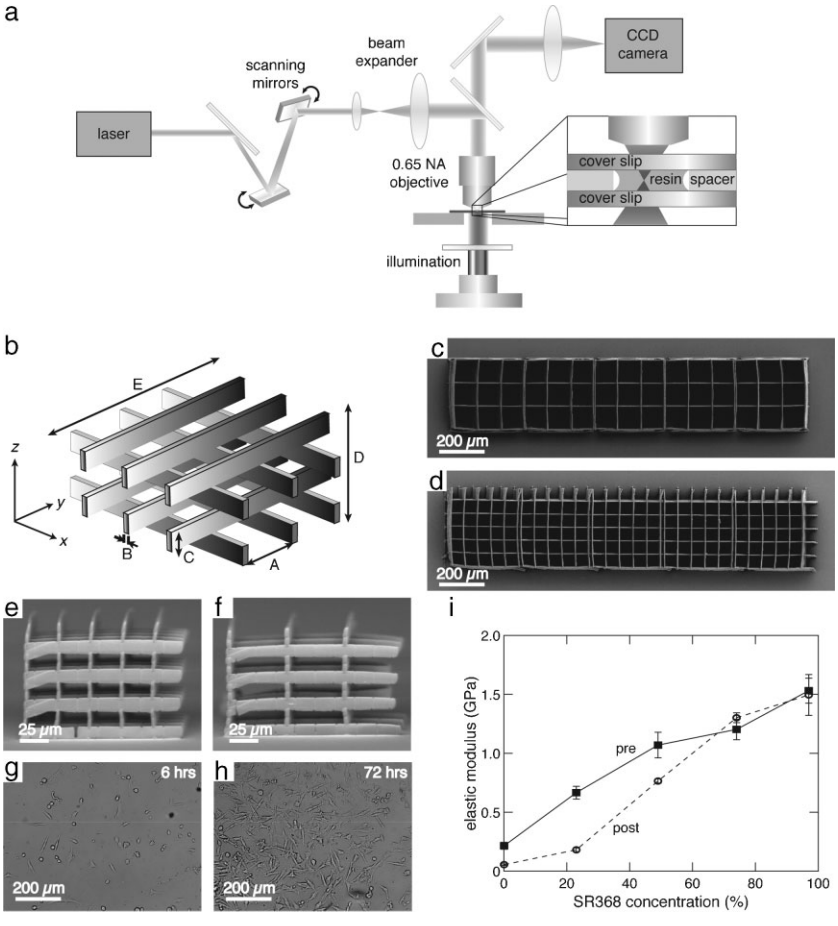

Figure 1. a) Schematic of the laser set-up used for fabrication. b) Schematic of the scaffold design illustrating different parameters of the scaffold. A = 12, 25, 52 or 110 μm; B = 5 μm; C = 12 μm; D = 100 μm; E = 375 μm. Top view scanning electron micrographs (SEM) of scaffolds with (c) 110-μm pore size and (d) 52-μm pore size. Side view SEM of (e) 25-μm and (f) 52-μm pore-sized scaffolds. Optical micrographs showing increase in the number of cells attached to a polymerized triacrylate 2D disc (g) 6 h and (h) 72 h after cell seeding. i) Bulk elastic modulus of UV photopolymerized triacrylate measured as a function of monomer concentration (solid line: before solvent treatment; broken line: after solvent treatment).

ADVANCED MATERIALS

long-term live cell imaging. Periodically, we filter out bright fluorescent cells from dim fluorescent population using fluorescence activated cell sorting to maintain overall high fluorescence intensity for long-term imaging.

We seed the fluorescently-labeled cells onto the scaffolds at a density of 500 000 cells mL^{-1}. Figure 2a shows a top-view bright-field image of cells taken 5 h after seeding inside a 52-μm pore-sized scaffold. Initially, the cells are located only on the cover slip, but start moving in 3D after a few hours. One day after cell seeding, we image the scaffolds using a 20× objective with a numerical aperture of 0.75 on a spinning-disc confocal microsope with a heated stage maintained at physiological conditions of 37 °C, 5% CO_2, and humidified atmosphere. For each experiment, we image z stacks (images with same xy positions but different z positions) at regular intervals. We record images in differential interference contrast and fluorescence imaging modes at 10-min intervals for a period of 8 h. To compare 2D and 3D migration, we prepare 2D films of UV polymerized triacrylate polymer on glass and treat them similarly for removal of monomer toxicity. We seed cells on the 2D substrates and image them in the same way as described above.

To track cell movement, we used commercial 3D imaging software. Based on the intensity and size of a cell, the software assigns it an x, y, and z coordinate at each instant. To characterize cell migration, we calculate the average speed, probability of movement, and motion persistence of the cells in the x, y, and z directions. Speed is defined as the sum of all the distances between subsequent images divided by the total time over which the imaging took place (10 min). Probability of movement is the number of imaging intervals during which the cell's displacement is larger than 1 μm divided by 48 (the total number of imaging intervals). Motion persistence is defined as the number of imaging intervals during which the cell's displacement is larger than 1 μm in the same direction for three consecutive time intervals divided by the total number of imaging intervals. This last parameter is a measure of the cell's tendency to continue moving in a certain direction.

We find that the cells readily move in three-dimensions inside the scaffold, as seen from a 3D-rendered image of GFP labeled cells (Fig. 2b) and the movie in Supporting Information. The cells attach and move predominantly along the beams in the 110-μm scaffold (Fig. 2c), while they occupy the entire pore in the smaller scaffolds (see movies in Supporting Information). Also, the cells are more uniformly dispersed inside the 52-μm scaffold than inside the 25- and 12-μm scaffold (Figs. 2d and 2f, respectively). Figure 3a depicts a typical track of the motion of a cell in a 25-μm scaffold. The overall mean speed of the cells is higher in the scaffold than it is on 2D substrate (Fig. 3b), but the lateral speed and persistence in the x and y directions are the same (Fig. 3c). In contrast, Figure 3d shows that the probability of movement in the x and y directions is lower in the scaffold than it is on 2D substrate, where cells encounter fewer obstructions. As the pore size is increased, the overall mean speed increases, but the persistence and probability of movement remain the same.

The higher value of the overall mean cell speed 3D compared to that in 2D is likely due to the additional degree of freedom for cell movement (Fig. 3b). In contrast, for collagen matrices the cell migration speed is lower in 3D than it is on a 2D substrate.[26] The collagen has pore sizes from nanometers to micrometers, but is degradable and softer than our matrix system. To migrate through the collagen matrix, the cells must therefore degrade the collagen or modify their shape. Our scaffolds, on the other hand, are stiff non-degradable polymer matrices that do not allow matrix proteolysis and only allow cell shape change and adhesion-deadhesion events for any movement.

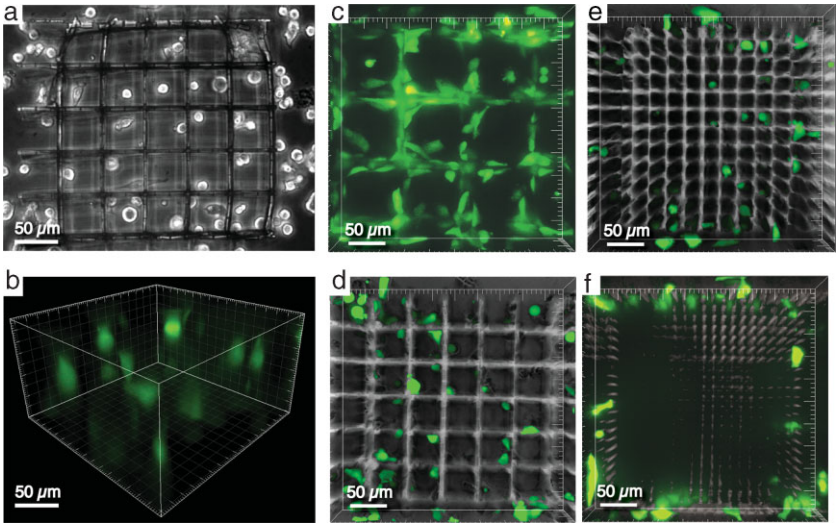

Figure 2. a) Brightfield optical image showing top view of cells inside a 52-μm pore-sized scaffold 5 h after of seeding cells. b) Fluorescence image showing isometric 3D rendered view of HT1080 cells inside a scaffold 24 h after seeding cells c-f) Top view overlay of fluorescence and differential interference contrast images of cells in 110, 52, 25 and 12-μm pore-sized scaffolds showing non-uniformity in the distribution of cells in different matrices owing to variations in physical obstruction.

The random-motion track in Fig. 3a confirms the interconnectedness of the 3D scaffolds and shows that the cell has freedom of movement along all three coordinate axes for a scaffold with pore size of 25 μm. However, the decrease in cell distribution uniformity with pore size observed in Figs. 2c–f indicates that the matrix obstructs the cells and prevents their free movement inside smaller pore-size scaffolds. The monotonic increase in overall mean speed with pore size (Fig. 3b) supports this interpretation. Earlier studies of collagen matrices show that pore size decreases as collagen concentration increases.[8,27,28] Modeling suggests that the cell speed should depend parabolically on pore size with a maximum at a pore size of

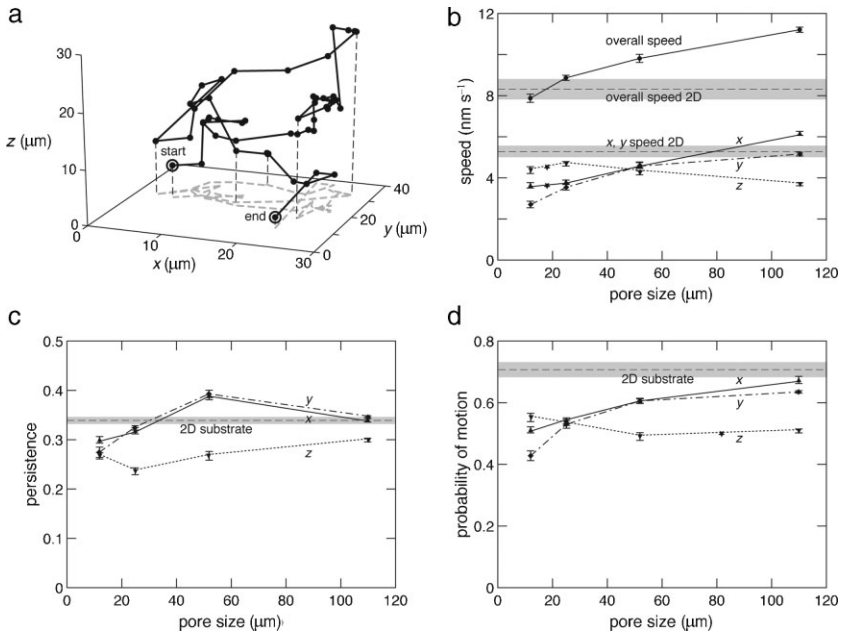

Figure 3. a) Typical track of a cell in a 25-μm scaffold. b) Overall mean speed and directional speed, (c) persistence and (d) probability of movement as a function of pore size. Data points: 3D matrices; dashed lines: values obtained on 2D substrates. The error bars represent the standard error around the mean value. Statistical significance was evaluated for difference in values between adjacent pore-sized scaffolds. It was also evaluated between 2D and 110-μm pore-sized scaffold. The difference between adjacent data points has p values of less than 0.05 for all pairs except those marked by an asterisk (*).

approximately 25 μm.[28] We do not see such a parabolic trend; instead cell speed continues to increase up to the largest pore size (110 μm), where the cells predominantly migrate along beams (Fig. 2c) without encountering many obstructions. Contrary to the prediction of models for a non-degradable matrix,[8,28] the migration speed of the cells in the 12-μm pore-sized scaffold is not zero. We observe that the cells change their shape and manage to squeeze through small pores (see Supporting Information), in accordance with observations by Wolf et al.[5]

To summarize, we developed a model three-dimensional (3D) extracellular matrix that provides precise and independent control of architectural parameters and that can be used for controlled cell adhesion and migration studies. We find that the 3D environment produces higher cell speeds than a 2D substrate. As the pore size of the 3D matrix is decreased, we observe a decrease in mean speed due to obstruction from the matrix. The fabrication and analysis techniques we describe in this paper open the door to systematic studies of the effects of mechanical properties, adhesion peptide concentration, and biodegradability on cell migration in three-dimensional environments.

Experimental

Materials: We purchased triacrylate monomers tris (2-hydroxy ethyl) isocyanurate triacrylate (SR368) and ethoxylated (6) trimethylolpropane triacrylate (SR499) from Sartomer Company, Inc and the photoinitiator, Lucirin-TPOL from BASF. We purchased the cell line HT1080 from ATCC. Invitrogen supplied all the cell culture media. We purchased the GFP plasmid from Clontech.

Scaffold Fabrication: We clean a cover-glass and silanize it with acryloxy-propyl-trimethoxy silane to facilitate the adhesion of a polymerized triacrylate film on the glass surface. The composition of liquid resin used for photopolymerization is a 48:49 ratio of the two triacrylate monomers SR368 and SR499, respectively, and 3% of the photoinitiator Lucirin-TPOL. We spin coat a thin film of the resin on a silanized cover-glass and polymerize it under a UV lamp for 10 min. We use this sample for 2D cell migration studies. For fabrication of 3D scaffolds, we place a drop of resin on a silanized acrylate-coated cover glass positioned on a sample stage and irradiate it with 130-fs, 800-nm laser pulses from a Ti-sapphire laser oscillator operating at a 80 MHz repetition rate (Fig. 1a). We use a 40× objective with numerical aperture 0.65 to focus the laser beam inside the resin. We fabricate the scaffolds by scanning the laser beam using a pair of galvanometer mirrors and moving the computer-controlled sample stage in the x, y and z directions. An increase in the index of refraction (1.522 *vs*. 1.493) of the polymer after photopolymerization allows visualizing the fabrication process with a charge coupled device camera using transmitted white light. The unpolymerized resin is washed off in ethanol leaving behind the 3D microfabricated scaffolds.

Mechanical Characterization: The bulk mechanical stiffness of the photopolymer is measured in a tensile testing machine. The specimen for the tensile test is a ''dog-bone'' shaped specimen made by polymerizing the liquid monomer/s under UV light for 10 min using a silicone mold sandwiched between two glass plates. The shape and dimensions of the dog-bone complies with ISO 527-2 for plastics and measures 75 mm long with the center section 5 mm wide by 1 mm thick by 30 mm long. We test three samples for each composition to add statistical significance to the measurements. We do the tests before and after solvent treatment to study the effect of the leaching of unpolymerized monomers on the mechanical stiffness of the photopolymer.

Cell Culture: We culture HT1080 fibrosarcoma cells in Eagle's Minimum Essential Medium (EMEM) supplemented with 10% fetal bovine serum (FBS) and 1% antibiotics (penicillin and streptomycin).

Cell Compatibility: We use silicone isolators as molds sandwiched between two glass slides to UV polymerize the triacrylate resin in the shape of discs 20 mm in diameter and 1 mm thick. We keep these discs in methanol placed on a shaker for 3 days to leach out the unpolymerized, toxic monomer. Then we place these polymer discs inside a non-tissue culture treated 12 well plate and seed HT1080 fibrosarcoma cells at a density of 100 cells per mm^2. We monitor cell growth by taking images every few hours and measure cell proliferation by detaching the cells using trypsin and counting them at different times using a cell counter. Same procedure of solvent leaching is used for 2D substrates and 3D scaffolds.

GFP Transfection: For transfection of cells, we seed 5×10^5 cells in a six-well plate in an EMEM medium with 10% FBS without any antibiotics. We dilute 2 μg of GFP plasmid in 250 μL of low serum medium (Optimem) and 2.5 μL of Lipofectamine-2000 in another 250 μL Optimem. We mix the two solutions and incubate them at room temperature for 45 min to allow lipid-DNA complexes to form. After 24 h, we replace the cell medium with 500 μL Optimem and add the lipid-DNA complex to each well. After incubating the cells for 5 h at

ADVANCED MATERIALS

37 °C in a 5% CO_2 incubator, we add medium with 10% FBS to the cells and allow them to incubate for another 24–36 h. At the end of 36 h, we sort and resort the cells a few times using a fluorescence assisted cell-sorting instrument to obtain a transient GFP-transfected population of cells.

Cell Migration Studies: We seed the scaffolds at a cell density of 500,000 cells/mL and allow the cells to attach and proliferate for 24 h before starting live imaging. Using 3D rendering and tracking software Imaris from Bitplane, Inc, we analyze the 3D time-lapse images for each experiment. After we adjust the overall threshold of the image, the software assigns coordinates to each cell and tracks them over time. From these data we obtain the overall mean speed and the speed in the x, y, and z directions. In calculating values for persistence and probability of movement of cells, we set a threshold value of 1 μm to differentiate between moving and non-moving cells. This value is well above the minimum temporal and spatial resolution of the imaging system.

Received: May 13, 2008
Revised: August 21, 2008
Published online: October 15, 2008

[1] S. Even-Ram, K. M. Yamada, *Curr. Opin. Cell Biol.* **2005**, *17*, 524.
[2] R. B. Dickinson, R. T. Tranquillo, *AiChE J.* **1993**, *39*, 1995.
[3] B. D. Harms, G. M. Bassi, A. R. Horwitz, D. A. Lauffenburger, *Biophys. J.* **2005**, *88*, 1479.
[4] E. Cukierman, R. Pankov, D. R. Stevens, K. M. Yamada, *Science* **2001**, *294*, 1708.
[5] K. Wolf, I. Mazo, H. Leung, K. Engelke, U. H. von Andrian, E. I. Deryugina, A. Y. Strongin, E. B. Brocker, P. Friedl, *J. Cell Biol.* **2003**, *160*, 267.
[6] P. Friedl, K. Wolf, *Nat. Rev. Cancer* **2003**, *3*, 362.
[7] F. Grinnell, L. B. Rocha, C. Iucu, S. Rhee, H. M. Jiang, *Exp. Cell Res.* **2006**, *312*, 86.
[8] M. H. Zaman, L. M. Trapani, A. Siemeski, D. MacKellar, H. Y. Gong, R. D. Kamm, A. Wells, D. A. Lauffenburger, P. Matsudaira, *Proc. Natl. Acad. Sci. USA* **2006**, *103*, 10889.
[9] C. Melani, M. Campana, B. Lombardot, B. Rizzi, F. Veronesi, C. Zanella, P. Bourgine, K. Mikula, N. Peyriéras, A. Sarti, *Conf. Proc. IEEE Eng. Med. Biol. Soc.* **2007**, *2007*. 1631.
[10] S. N. Bhatia, U. J. Balis, M. L. Yarmush, M. Toner, *Biotechnol. Prog.* **1998**, *14*, 378.
[11] C. S. Chen, M. Mrksich, S. Huang, G. M. Whitesides, D. E. Ingber, *Science* **1997**, *276*, 1425.
[12] C. K. Chua, K. F. Leong, C. M. Cheah, S. W. Chua, *Int. J. Adv. Manuf. Technol.* **2003**, *21*, 291.
[13] D. W. Hutmacher, *Biomaterials* **2000**, *21*, 2529.
[14] E. Sachlos, J. T. Czernuszka, *Eur. Cell. Mater.* **2003**, *5*, 29.
[15] P. Sarazin, X. Roy, B. D. Favis, *Biomaterials* **2004**, *25*, 5965.
[16] T. Weigel, G. Schinkel, A. Lendlein, *Expert Rev. Med. Devices* **2006**, *3*, 835.
[17] D. W. Hutmacher, *J. Biomater. Sci. Polym. Ed.* **2001**, *12*, 107.
[18] M. H. Too, K. F. Leong, C. K. Chua, Z. H. Du, S. F. Yang, C. M. Cheah, S. L. Ho, *Int. J. Adv. Manufact. Technol.* **2002**, *19*, 217.
[19] A. Ovsianikov, B. Chichkov, O. Adunka, H. Pillsbury, A. Doraiswamy, R. J. Narayan, *Appl. Surf. Sci.* **2007**, *253*, 6603.
[20] M. P. Lutolf, J. A. Hubbell, *Nat. Biotechnol.* **2005**, *23*, 47.
[21] W. Denk, J. H. Strickler, W. W. Webb, *Science* **1990**, *248*, 73.
[22] B. H. Cumpston, S. P. Ananthavel, S. Barlow, D. L. Dyer, J. E. Ehrlich, L. L. Erskine, A. A. Heikal, S. M. Kuebler, I. Y. S. Lee, D. McCord-Maughon, J. Q. Qin, H. Rockel, M. Rumi, X. L. Wu, S. R. Marder, J. W. Perry, *Nature* **1999**, *398*, 51.
[23] S. Maruo, O. Nakamura, S. Kawata, *Opt. Lett.* **1997**, *22*, 132.
[24] T. Baldacchini, C. N. LaFratta, R. A. Farrer, M. C. Teich, B. E. A. Saleh, M. J. Naughton, J. T. Fourkas, *J. Appl. Phys.* **2004**, *95*, 6072.
[25] Z. Bayindir, Y. Sun, M. J. Naughton, C. N. LaFratta, T. Baldacchini, J. T. Fourkas, J. Stewart, B. E. A. Saleh, M. C. Teich, *Appl. Phys. Lett.* **2005**, *86*.
[26] S. Hazgui, N. Bonnet, J. Cutrona, B. Nawrocki-Raby, M. Polette, L. Chouchane, P. Birembaut, J. M. Zahm, *Am. J. Physiol. Cell Physiol.* **2005**, *289*, C1547.
[27] S. Sun, J. Wise, M. Cho, *Tissue Eng.* **2004**, *10*, 1548.
[28] M. H. Zaman, P. Matsudaira, D. A. Lauffenburger, *Ann. Biomed. Eng* **2007**, *35*, 91.